PAPER

Check for updates

Polytyrosine nanoparticles enable ultra-high loading of doxorubicin and rapid enzyme-responsive drug release†

Xiaolei Gu, Min Qiu, Huanli Sun, [ID] Jian Zhang, Liang Cheng, Chao Deng [ID] * and Zhiyuan Zhong [ID] *

Despite the great significance of clinically viable nanovehicles, very few of them exhibit stability and high anticancer drug loading with fast intracellular drug release. Herein, we report that polytyrosine nano-particles (PTNs) self-assembled from poly(ethylene glycol)-*b*-poly(L-tyrosine) block copolymer enable the ultra-high loading and rapid enzyme-responsive release of doxorubicin (DOX). Notably, PTNs achieve a remarkably high DOX loading of 63.1 wt% likely due to the existence of strong $\pi-\pi$ stacking between poly-tyrosine and DOX, as shown by UV-vis analysis. Additionally, PTNs present a high docetaxel loading of 17.5 wt%. Furthermore, PTNs exhibit good colloidal stability in 10% FBS, but are quickly de-stabilized by proteinase K. Interestingly, *ca.* 90% of DOX is released under 6 U mL^{-1} proteinase K in 24 h or in RAW 264.7 cells in 8 h. The DOX-loaded PTNs display efficient delivery and release of DOX in both RAW 264.7 cells and HCT-116 human colorectal cancer cells, achieving a better *in vitro* antiproliferative effect than the clinically used liposomal DOX formulation. Thus, these polytyrosine nanoparticles appear to be a potentially viable platform for the controlled delivery of anthraquinone anticancer agents.

1. Introduction

Nanoparticles self-assembled from amphiphilic biodegradable block copolymers are among the best vehicles for potent and clinically used lipophilic anthraquinone anticancer agents such as doxorubicin (DOX) and docetaxel (DTX).[1–3] However, nano-assemblies usually exhibit a moderate drug loading capacity, with drug loading contents typically less than 10 wt%.[4–6] Moreover, drug-loaded nanoparticles often exhibit inadequate *in vivo* stability, leading to premature drug release and pronounced adverse effects.[7,8] In the past years, various strategies such as chemical conjugation of drugs,[9–12] chemical crosslinking of nanoparticles,[13–15] and introduction of physical interactions such as hydrogen bonding, electrostatic inter-action, and $\pi-\pi$ stacking between carrier and loaded drug[16–18] have been exploited to enhance the drug loading levels and systemic stability of nanoparticles. Especially, the $\pi-\pi$ stacking approach by introducing phenyl, naphthyl, coumarin, and chrysin groups to hydrophobic blocks is particularly interesting.[19–22] For example, the poly(ethylene glycol)-poly(ε-caprolactone) (PEG-PCL) micelles formed following the conjugation of chrysin at the PCL terminal displayed a significantly enhanced loading content of DOX from 12.9% to 25.5%.[19] Hennink *et al.* reported that phenyl-modified poly(*N*-(2-hydroxypropyl)methacrylamide) micelles could achieve an efficient loading of DTX with a drug loading content of about 30 wt%, and DTX-loaded micelles resulted in complete regression of tumor xenografts in mice.[20] However, to obtain such a carrier, extra coupling reactions and purification procedures are generally required. Moreover, the existence of $\pi-\pi$ stacking between the carrier and loaded drug might also delay or reduce the drug release inside tumor cells, resulting in a compromised therapeutic effect.

Polypeptide-based nano-assemblies with versatile structures, excellent safety, and tunable degradability are one of the most studied nanoplatforms for cancer treatment and diagnosis.[23–27] Several polypeptide-based nanosystems carrying DOX (NK911), paclitaxel (NK105), and cisplatin (NC6004) have advanced into phase II and III clinical trials.[4] Notably, polypeptides that exhibit high stability against hydrolysis can be degraded by specific enzymes *in vivo*. For example, polypeptide hydrogels developed from polyalanine, polyphenylalanine, and poly(γ-ethyl-L-glutamate) were shown to exhibit the local sustained release of anticancer drugs and proteins as a result

Biomedical Polymers Laboratory, and Jiangsu Key Laboratory of Advanced Functional Polymer Design and Application, College of Chemistry, Chemical Engineering and Materials Science, Soochow University, Suzhou 215123, China.
E-mail: cdeng@suda.edu.cn, zyzhong@suda.edu.cn; Fax: +86-512-65880098;
Tel: +86-512-65880098
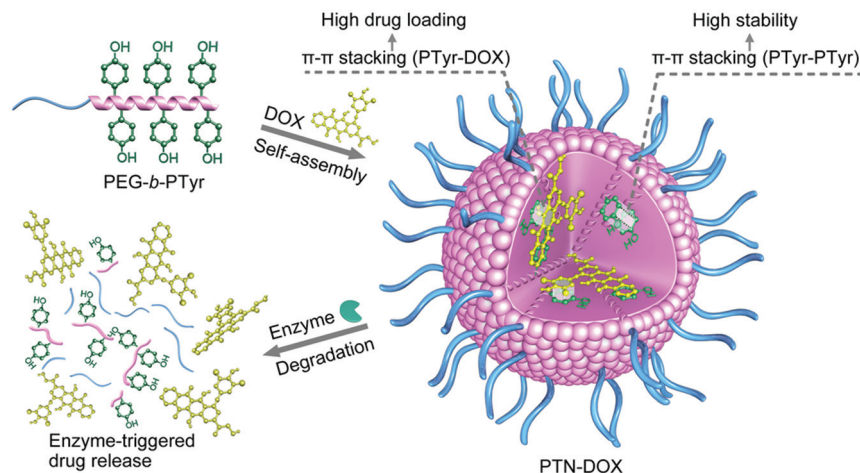
Scheme 1 Illustration of polytyrosine nanoparticles (PTNs) based on poly(ethylene glycol)-*b*-poly(L-tyrosine) block copolymer for ultra-high loading and rapid enzyme-responsive release of DOX.

of controlled enzymatic degradation.[28,29] Heise *et al.* reported that micelles and vesicles with hydrophilic poly(L-glutamic acid) coronas could be selectively degraded by elastase and thermolysin, causing nanoparticle destabilization and aggregation.[30]

Herein, we report polytyrosine nanoparticles (PTNs) self-assembled from poly(ethylene glycol)-*b*-poly(L-tyrosine) (PEG-*b*-PTyr) block copolymer for the ultra-high loading and rapid enzyme-responsive release of anthraquinone anticancer agents such as DOX (Scheme 1). PTyr blocks directly derived from the natural amino acid tyrosine possess pendant phenol groups on side chains, which significantly enhance the drug loading and stability of PTNs *via* π–π stacking. PEG2000-*b*-oligo(tyrosine) block copolymer was reported to form thermoresponsive, biodegradable and nontoxic hydrogels.[31] Our results show that DOX-loaded PTNs while stable under physiological conditions, achieve efficient delivery and release of DOX in both RAW 264.7 cells and HCT-116 human colorectal cancer cells, resulting in a superior antiproliferative effect to the clinically used liposomal DOX (LP-DOX) formulation. Thus, these simple, robust and enzyme-responsive polytyrosine nanoparticles offer an appealing platform for targeted cancer chemotherapy.

2. Experimental methods

2.1. Synthesis of PEG-*b*-PTyr copolymers

mPEG-*b*-PTyr copolymers were synthesized *via* the ring-opening polymerization (ROP) of Tyr-NCA monomer in DMF using PEG-NH$_2$ as an initiator. Under an N$_2$ atmosphere, a stock solution of PEG-NH$_2$ (500 mg, 0.1 mmol) in DMF (4 mL) was quickly added to a solution of Tyr-NCA (621 mg, 3 mmol) in DMF (3.8 mL). The reaction proceeded at 40 °C for 3 days, and the PEG-*b*-PTyr$_{30}$ product was recovered through precipitation in Et$_2$O and drying under high vacuum for 24 h. Yield: 89.0%. ^{1}H NMR (400 MHz, DMSO-d_6, δ): 9.10 (–OH), 6.94
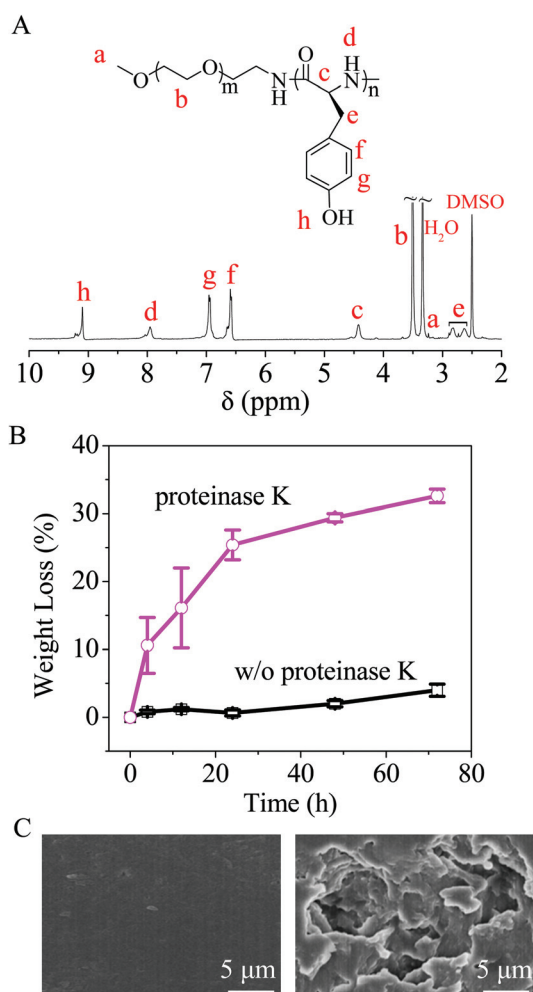
Fig. 1 Characteristics of the PEG-*b*-PTyr copolymer (Table 1, entry 1). (A) ^{1}H NMR spectrum (400 MHz, DMSO-d_6). (B) Weight loss of the polymer films with time in HEPES with or without proteinase K (120 U mL^{-1}) at 37 °C. (C) SEM micrographs of the polymer films following 72 h incubation at 37 °C in HEPES without (left) or with (right) proteinase K (120 U mL^{-1}).

$(-C_6H_2CH_2)$, 6.57 $(-C_6H_2OH-)$, 4.42 $(-COCHNH-)$, 2.82–2.63 $(-C_6H_4CH_2)$.

2.2. Preparation of polypeptide nanoparticles

PEG-*b*-PTyr nanoparticles (PTNs) were prepared *via* the drop-wise addition of HEPES buffer (pH 7.4, 10 mM, 900 μL) to a DMF solution of PEG-*b*-PTyr copolymers (5 mg mL^{-1}, 100 μL) under stirring at room temperature followed by extensive dialysis against HEPES for 8 h (MWCO 7000 Da). The medium was refreshed every 1 h. The size and zeta potential of PTNs were measured by dynamic light scattering (DLS) and electrophoresis, respectively. The critical aggregation concentration (CAC) of PTNs was determined using pyrene as a fluorescence probe.

The enzymatic responsivity of PTNs was measured by incubation with proteinase K (6 U mL^{-1}) in HEPES (10 mM, pH 7.4) at 37 °C with shaking, and the hydrodynamic diameter was monitored by DLS.

2.3. Enzyme-triggered release of DOX

For *in vitro* drug release, PTN-DOX was placed in a dialysis tube (MWCO 12 000) at a micelle concentration of 0.1 mg mL^{-1} under shaking at 37 °C in two different media: (i) HEPES (10 mM, pH 7.4) and (ii) HEPES (10 mM, pH 7.4) containing proteinase K (6 U mL^{-1}). Typically, 0.6 mL of PTN-DOX dispersion was dialyzed against HEPES buffer (10 mM, pH 7.4, 25 mL). At predetermined intervals, 5.0 mL of release medium

Table 1 Synthesis of PEG-*b*-PTyr copolymers

		M_n (kg mol^{-1})				
Entry	Copolymer	Design	^{1}H NMR^a	GPC^b	M_w/M_n ^{b}	Yield (%)
1	PEG-*b*-PTyr$_{30}$	5–4.9	5–4.9	9.1	1.08	89
2	PEG-*b*-PTyr$_{62}$	5–9.8	5–10.1	14.9	1.06	91
3	PEG-*b*-PTyr$_{90}$	5–16.3	5–14.7	19.0	1.20	85

^{a} Calculated from ^{1}H NMR (DMSO-d_6). ^{b} Determined by GPC (eluent: DMF and standard : polystyrene).
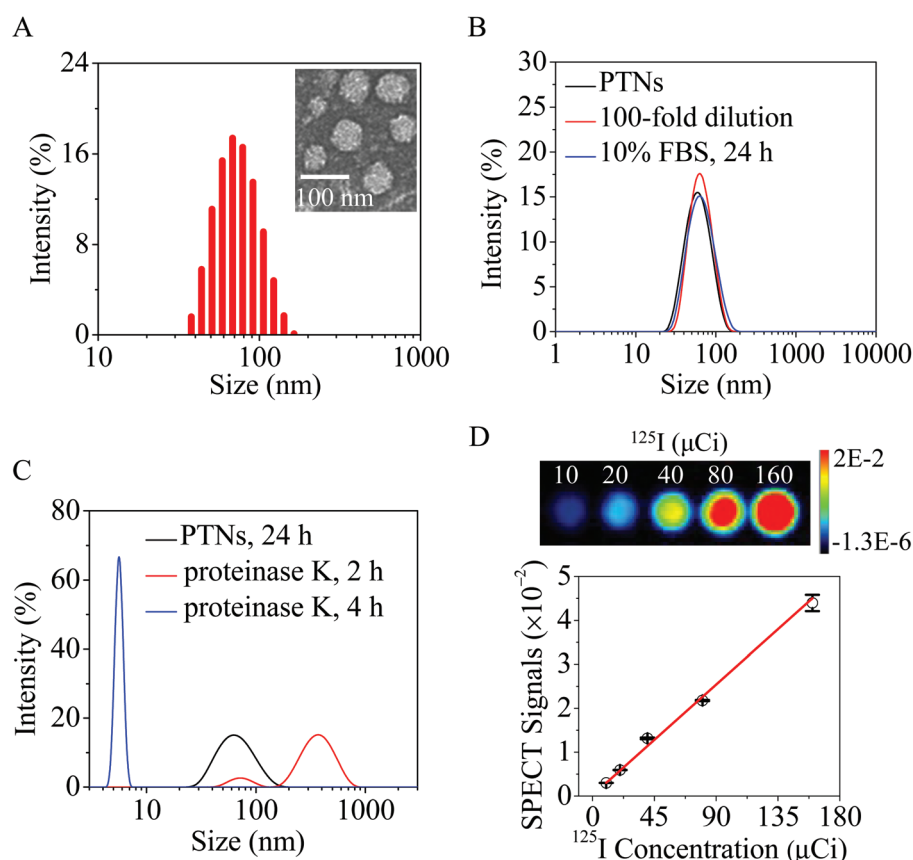
Fig. 2 Characterization of PTNs. (A) Size distribution of PTNs measured by DLS and TEM. (B) Colloidal stability of PTNs measured by DLS. (C) Size change profiles of PTNs (0.5 mg mL^{-1}) in response to proteinase K (6 U mL^{-1}) in HEPES at 37 °C. (D) *In vitro* SPECT signals of ^{125}I-labeled PTNs (^{125}I-PTNs) at varying ^{125}I concentrations in the range of 10–160 μCi.

was withdrawn and refilled with fresh medium. The DOX in the release medium was quantified by fluorescence measurement (FLS920). The release experiments were conducted in triplicate, and the results presented as mean ± SD.

2.4. Intracellular release of DOX

The intracellular drug release from PTN-DOX was evaluated in RAW 264.7 cells according to our previous report.[32] Briefly, PTN-DOX in 200 μL HEPES (100 μg DOX per mL) was incubated with the cells in a 6-well plate for 4 h. The culture medium was collected, and the amount of drug remaining in the culture medium (W_1) was determined by fluorescence measurement. The cells following incubation in fresh medium for predetermined times (4 h, 6 h and 8 h) were harvested and lysed with 1% Triton X-100 under ultrasound for 20 min. The supernatant was collected by centrifugation and dialyzed for 4 h to remove the free drug. A control experiment with PTN-DOX showed 20% drug loss during the lysis of cells, centrifugation, and dialysis. The DOX remaining in the PTNs (W_2) was extracted using DMF and re-adjusted accordingly. The amount of released drug in the cells was calculated according to the following formula based on the calibration curve obtained with DOX/DMF of known DOX concentrations:

$$\text{Drug released in the cells } (\%) = (W_0 - W_1 - W_2)/W_0 \times 100$$

where, W_0 refers to the total weight of added drug.

3. Results and discussion

3.1. Preparation and characterization of amphiphilic PEG-b-PTyr copolymers

PEG-b-PTyr copolymers were readily obtained via the polymerization of L-tyrosine N-carboxyanhydride (L-Tyr-NCA) using PEG-NH$_2$ (M_n = 5.0 kg mol^{-1}) as an initiator (Scheme S1†). The ^{1}H NMR spectrum of PEG-b-PTyr displays the characteristic signals of PEG (δ 3.56 and 3.24) and PTyr (δ 9.10, 6.94, 6.57, 4.42, 2.82 and 2.63) (Fig. 1A). The M_n of the PTyr block was calculated by comparing the integrals of the signals at δ 6.94 (benzyl protons of the tyrosine moieties) and δ 3.56 (methylene protons of PEG). The results reveal that all three PEG-b-PTyr copolymers had an M_n close to our design (Table 1). The GPC

analyses further reveal that the PEG-b-PTyr copolymers had prescribed molecular weights and a narrow molecular weight distribution ($Đ$ = 1.06–1.2) (Table 1). The FTIR spectrum of PEG-b-PTyr displays signals at 1650 cm^{-1} (v_{NHCO}, amide I) and 1550 cm^{-1} (v_{NHCO}, amide II) (Fig. S1†), which are the characteristic signals of the α-helical conformation.[33,34] It is known that
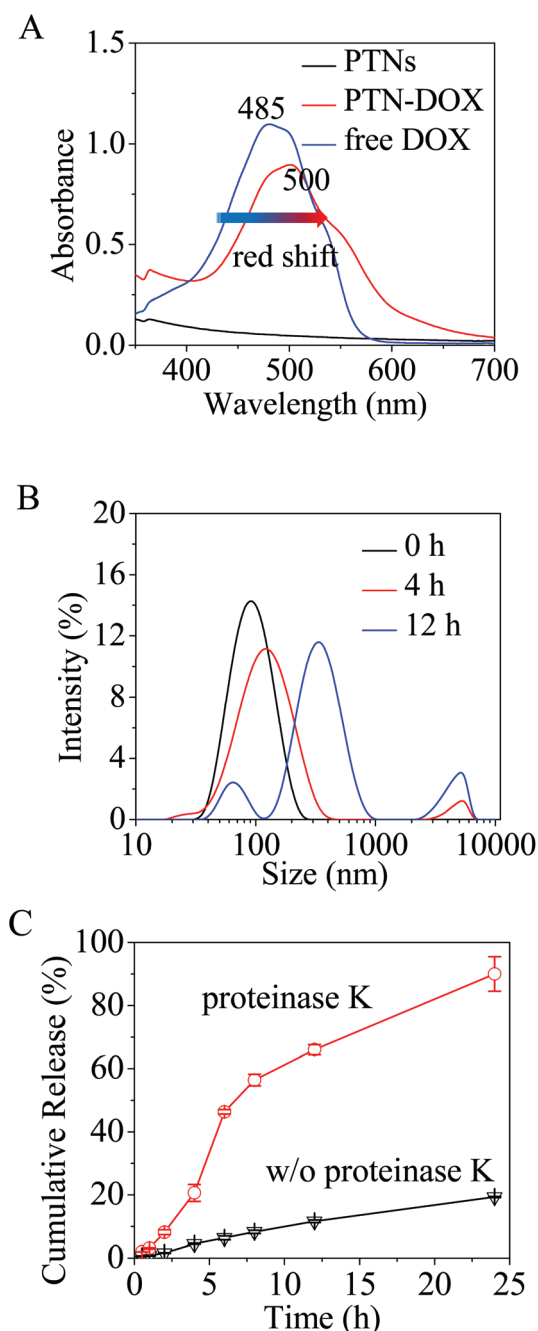
Fig. 3 Characterization of DOX-loaded PTNs (PTN-DOX, Table 2, entry 2). (A) UV-Vis spectra of PTNs, PTN-DOX, and DOX, where the concentration of DOX was 100 μg mL^{-1}. (B) Size change profiles of PTN-DOX (0.5 mg mL^{-1}) in response to proteinase K (6 U mL^{-1}) in HEPES at 37 °C. (C) In vitro release of DOX in the presence or absence of proteinase K (6 U mL^{-1}) from PTN-DOX (0.1 mg mL^{-1}).

Table 2 Characteristics of PTN-DOX

Entry	DLC (wt%) Theory	DLC (wt%) Determined[a]	DLE[a] (%)	Size[b] (nm)	PDI[b]	Zeta[c] (mV)
1	20	19.1	94.5	97	0.16	−3.8
2	30	27.9	89.9	111	0.16	−3.4
3	40	37.5	89.5	126	0.15	−3.4
4	50	46.6	87.3	134	0.22	−3.1
5	60	56.2	85.6	162	0.19	−2.4
6	70	63.1	73.2	181	0.23	−1.1

[a] Determined by fluorescence measurement. [b] Determined by DLS analysis. [c] Measured by electrophoresis.

polypeptides and proteins are prone to proteolytic degradation inside cells. The abundant enzymes in lysosomes can digest different polypeptides and proteins. Here, we investigated the proteolytic degradation of PEG-*b*-PTyr copolymer *in vitro* using proteinase K, which is commonly used in molecular biology for protein degradation and in materials science for polymer biodegradation[35,36] as a model protease. Interestingly, the PEG-*b*-PTyr copolymer films exhibited high stability in HEPPS buffer, as evidenced by the slight weight loss and intact film surface following 72 h incubation (Fig. 1B and C). On the contrary, the PEG-*b*-PTyr films treated with proteinase K displayed over 30 wt% weight loss and a cracked morphology, signifying their enzymatic degradability.

3.2. Fabrication of polytyrosine nanoparticles (PTNs), drug loading, and enzyme-triggered drug release

PEG-*b*-PTyr copolymer with an M_n of 5.0–4.9 kg mol^{-1} (Table 1, entry 1) was employed to fabricate polytyrosine nanoparticles

(PTNs) *via* the solvent exchange method. The DLS and TEM measurement show that PTNs have a small hydrodynamic diameter of 76 nm, a spherical morphology, and low polydispersity (PDI = 0.10) (Fig. 2A). Notably, PTNs display a low CAC of 8.9 mg L^{-1} and high stability against dilution and 10% FBS (Fig. 2B). Interestingly, in the presence of proteinase K (6 U mL^{-1}) in HEPES (pH 7.4, 10 mM) at 37 °C, PTNs firstly swelled and then completely dissociated into unimers in 4 h (Fig. 2C), signifying their fast enzymatic degradation. This fast degradation was not anticipated given that PTyr is located in the micellar core. A plausible reason for this is that the PTyr block is amphipathic, which allows good enzyme accessibility. The tyrosine moieties in proteins have widely been employed for radioactive labeling with iodine.[37–39] Given its abundant tyrosine units, we also investigated the labeling of the PEG-*b*-PTyr copolymer with radioactive ^{125}I. The results display the facile radioactive labeling of the PEG-*b*-PTyr copolymer and preparation of ^{125}I-labeled nanoparticles (^{125}I-PTNs). *In vitro* SPECT/
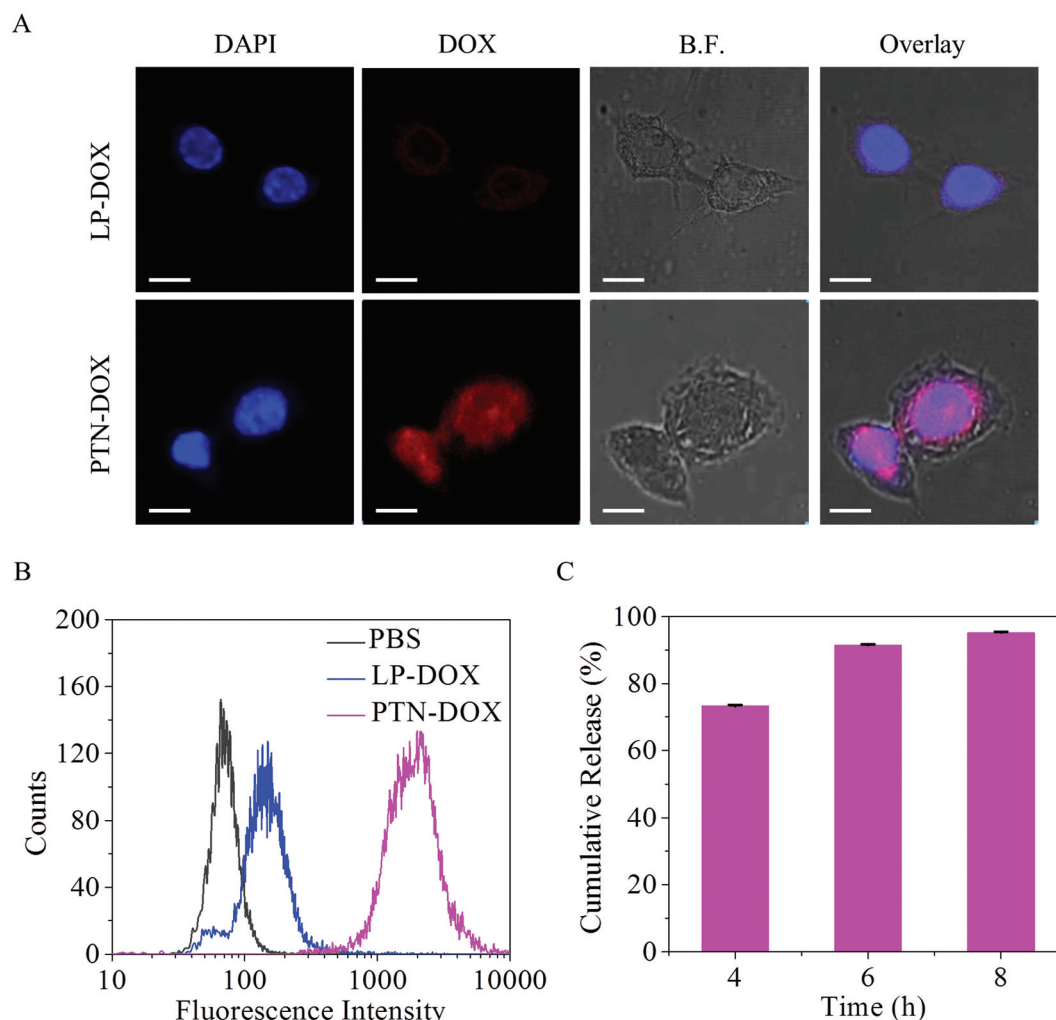
Fig. 4 Cellular uptake and intracellular drug release of PTN-DOX in RAW 264.7 cells. (A) CLSM images of cells treated with PTN-DOX and LP-DOX (DOX dosage: 20.0 μg mL^{-1}) for 8 h. Scale bar, 20 μm. (B) Flow cytometry analysis. Cells were treated with PTN-DOX and LP-DOX (DOX dosage: 5.0 μg mL^{-1}) for 4 h. (C) Intracellular drug release profiles (DOX dosage: 100 μg mL^{-1}).

CT imaging shows that ^{125}I-PTNs give strong radioactive images, in which the intensities of the SPECT signals increase linearly with and increase in ^{125}I levels in PTNs (Fig. 2D). Thus, ^{125}I-PTNs have great potential for revealing in the vivo fate of nanoparticles and diagnosis.[40–43]

Remarkably, PTNs displayed an extremely efficient loading of DOX with drug loading contents reaching as high as 63.1 wt% (Table 2). To the best of our knowledge, this represents the highest DOX loading ever reported for polymeric micelles. Polymeric nanomedicines have a typical drug loading capacity of around 10 wt%.[44,45] This high drug loading is advantageous because it would significantly reduce the amount of carrier materials and dosing volume of nanomedicines.[46–48] The high drug loading capacity of PTNs is mainly attributed to the strong π–π stacking between DOX and the tyrosine units located in the micellar core, as also reported for other π–π stacking nanosystems.[22,49,50] The π–π stacking between DOX and the PTyr segments was evidenced by a pronounced red-shift of 15 nm in the DOX-loaded PTNs (PTN-DOX) relative to free DOX (Fig. 3A). The size of PTN-DOX increased from 97 to 181 nm with an increase in DOX loading content from 19.1 to 63.1 wt% (Table 2). All the PTN-DOX had a slightly negative charge (−3.8 to −1.1 mV) and were quickly swollen under proteinase K (Fig. 3B). The *in vitro* release studies display that the drug release from PTN-DOX was significantly suppressed under enzyme-free conditions, while about 90% of DOX was released in 24 h in HEPES containing proteinase K (6 U mL^{-1}) (Fig. 3C). These results indicate that PTN can be readily degraded by proteinase K, which is likely due to the fact that the core-forming PTyr is amphipathic, allowing good accessibility of proteinase K. We further studied the loading of DTX, another anthraquinone anticancer agent, in PTNs. The results show a high DTX loading content of 17.5 wt% (Table S1†), which is significantly higher than previously reported for DTX nanoformulations (typically lower than 8 wt%).[51–53] A greatly enhanced DTX loading was also observed in phenyl-modified poly(N-(2-hydroxypropyl) methacrylamide) micelles.[49]

3.3. Intracellular drug release and inhibitory effect of PTN-DOX in RAW 264.7 cells

RAW 264.7 macrophage cells were employed as model cells to evaluate the intracellular drug release and inhibitory effect of PTN-DOX because they possess efficient uptake of nanoparticles. Moreover, macrophage cells are also reported to associate with many diseases including inflammatory diseases, atherosclerosis, cancer, and diabetes.[54–57] The CLSM images reveal strong DOX fluorescence in the nuclei of cells following 8 h incubation with PTN-DOX, while weak DOX fluorescence was noticed in the cells treated with the clinically used LP-DOX (Fig. 4A). Flow cytometry showed that the cells treated with PTN-DOX had a higher DOX fluorescence level by more than ten times that with LP-DOX (Fig. 4B). We further studied the intracellular drug release of PTN-DOX in RAW 264.7 cells. Fig. 4C reveals that about 70% and 90% of DOX was released from PTN-DOX in the cells in 4 and 8 h, respectively. These

results confirm that PTN is prone to fast proteolytic degradation inside cells, leading to efficient intracellular drug release.

Remarkably, the MTT assays demonstrated that PTN-DOX induced a high antiproliferative activity to RAW 264.7 cells
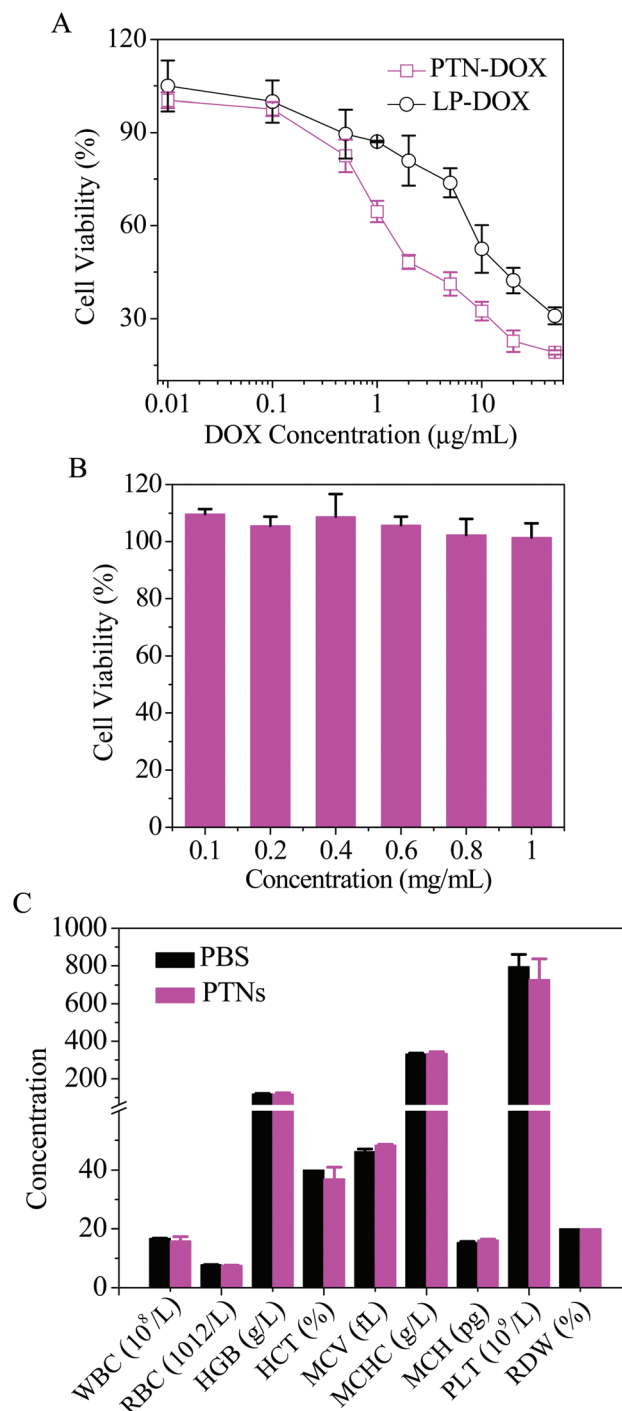
Fig. 5 *In vitro* antiproliferative activity and hematology analysis of PTN-DOX. (A) MTT assays of PTN-DOX and LP-DOX against RAW 264.7 cells. (B) MTT assays of blank PTNs in RAW 264.7 cells following 48 h incubation. (C) Hematology analysis of Kunming mice after intravenous administration of PBS and PTNs (dose: 50 mg kg^{-1}).
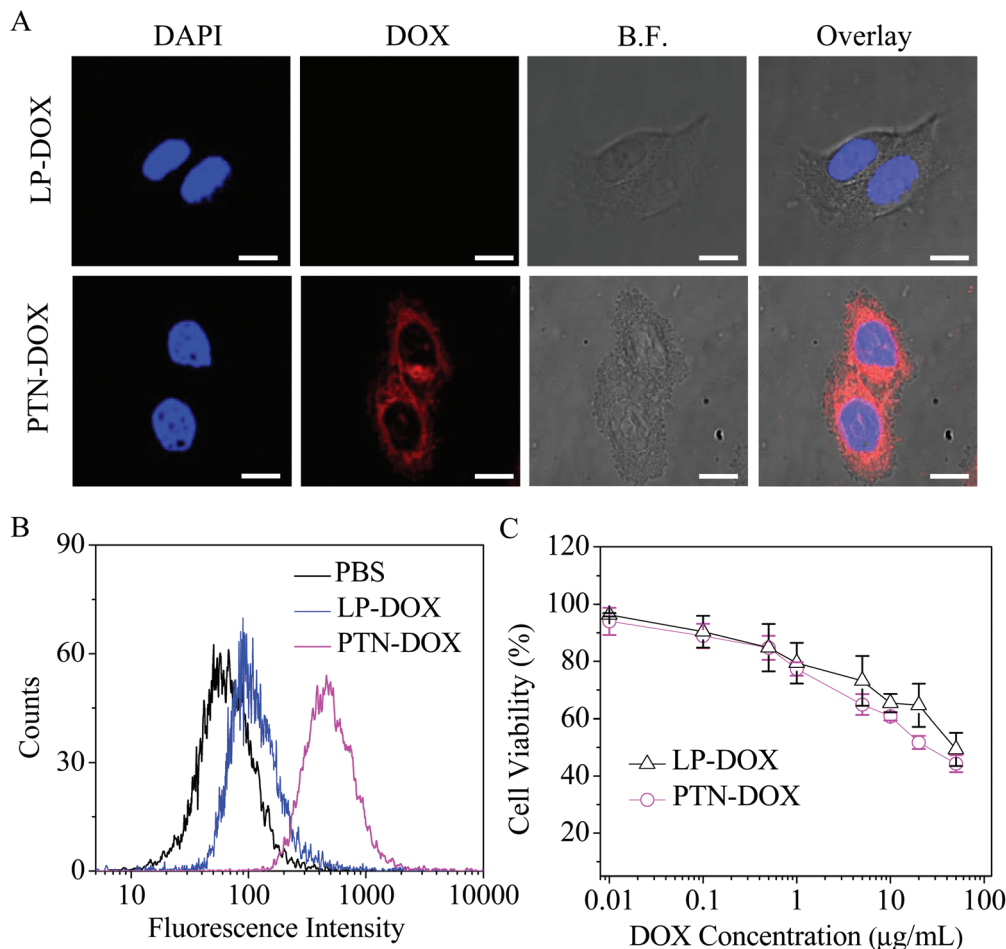
Fig. 6 Cellular uptake and *in vitro* antitumor activity of PTN-DOX in HCT-116 human colorectal cancer cells. (A) CLSM images of HCT-116 cells treated with PTN-DOX (DOX dosage: 20.0 μg mL^{-1}) for 8 h. Scale bar: 20 μm. (B) Flow cytometry analysis of HCT-116 cells following 4 h incubation with PTN-DOX (DOX dosage: 5.0 μg mL^{-1}). (C) MTT assays. The cells were treated with PTN-DOX for 4 h and then incubated in fresh medium for another 68 h. LP-DOX was used as a control.

with a half maximal inhibitory concentration (IC$_{50}$) of 3.0 μg DOX equiv. per mL, which is about 5-fold lower than that of LP-DOX (Fig. 5A). Importantly, both the RAW 264.7 cells (Fig. 5B) and L929 cells (Fig. S2†) treated with blank PTNs for 48 h at concentrations in the range of 0.1–1 mg mL^{-1} displayed almost 100% cell viability, which confirms that these polytyrosine nanoparticles are non-cytotoxic. Furthermore, routine blood examinations revealed that the administration of blank PTNs had little influence on the levels of white blood cells, red blood cells, hemoglobin, and platelets in mice (Fig. 5C), corroborating that PTNs have excellent biocompatibility.

3.4. Cellular uptake and antitumor activity of PTN-DOX in HCT-116 human colorectal cancer cells

We further evaluated the cellular uptake and intracellular drug release behaviors of PTN-DOX using HCT-116 human colorectal cancer cells. Notably, strong DOX fluorescence was observed in the perinuclei area of the HCT-116 cells following 8 h incubation with PTN-DOX, which confirms its effective

internalization and drug release in cancer cells (Fig. 6A). In comparison, the HCT-116 cells treated with LP-DOX displayed slight DOX fluorescence. It should further be noted that the HCT-116 cancer cells treated with PTN-DOX had comparably weaker intracellular DOX fluorescence than the RAW 264.7 cells under the same conditions, which is likely due to their less efficient uptake of PTN-DOX. Macrophage cells with the innate phagocytic capability are known to exhibit better uptake of nanoparticles than normal cells.[58,59] Flow cytometry corroborated that the PTN-DOX treated HCT-116 cells had a significantly higher cellular DOX fluorescence intensity than the LP-DOX treated cells (Fig. 6B), which is most likely due to the fact that PTN-DOX releases DOX faster inside the cells as a result of proteolytic degradation. The MTT assays demonstrated that PTN-DOX induced high antitumor activity in the HCT-116 cells with an IC$_{50}$ value of 20.4 μg DOX equiv. per mL, which is approximately two times lower than that of LP-DOX (40.2 μg DOX equiv. per mL) (Fig. 6C). It should be further noted that PTNs are amenable to surface functionalization with varying targeting ligands such as peptides, anti-

bodies, and polysaccharides, which will significantly enhance target cancer cell uptake and the anticancer effect.[60,61] Thus, these robust and enzyme-responsive polytyrosine nanoparticles, which simultaneously exhibit a high anticancer drug loading and fast intracellular drug release, provide a valuable platform for targeted cancer chemotherapy.

4. Conclusion

We have demonstrated that polytyrosine nanoparticles (PTNs) self-assembled from PEG-PTyr block copolymer achieve ultra-high loading and rapid enzyme-responsive release of DOX. Intriguingly, the DOX-loaded PTNs (PTN-DOX) exhibit small sizes, narrow polydispersity, good colloidal stability, and ultra-high drug loading content up to 63.1 wt%, which is likely due to the strong π–π stacking between polytyrosine and the drug. Remarkably, PTN-DOX while largely suppressed the leakage of DOX under physiological conditions could achieve fast drug release in RAW 264.7 cells or in the presence of proteinase K, resulting in an enhanced antiproliferative effect compared with the clinically used LP-DOX in both RAW 264.7 cells and HCT-116 human colorectal cancer cells. Thus, these robust and enzyme-responsive polytyrosine nanoparticles are highly promising for targeted cancer chemotherapy.

Conflicts of interest

There are no conflicts to declare.

Acknowledgements

References

1 H. Chen, W. Zhang, G. Zhu, J. Xie and X. Chen, *Nat. Rev. Mater.*, 2017, **2**, 17024.

2 N. Kamaly, B. Yameen, J. Wu and O. C. Farokhzad, *Chem. Rev.*, 2016, **116**, 2602–2663.

3 Z. Tang, C. He, H. Tian, J. Ding, B. S. Hsiao, B. Chu and X. Chen, *Prog. Polym. Sci.*, 2016, **60**, 86–128.

4 H. Cabral and K. Kataoka, *J. Controlled Release*, 2014, **190**, 465–476.

5 K. Y. Choi, H. Y. Yoon, J.-H. Kim, S. M. Bae, R.-W. Park, Y. M. Kang, I.-S. Kim, I. C. Kwon, K. Choi, S. Y. Jeong, K. Kim and J. H. Park, *ACS Nano*, 2011, **5**, 8591–8599.

6 W. Chen, F. Meng, R. Cheng, C. Deng, J. Feijen and Z. Zhong, *J. Controlled Release*, 2015, **210**, 125–133.

7 M. Talelli, M. Barz, C. J. F. Rijcken, F. Kiessling, W. E. Hennink and T. Lammers, *Nano Today*, 2015, **10**, 93–117.

8 C. Deng, Y. Jiang, R. Cheng, F. Meng and Z. Zhong, *Nano Today*, 2012, **7**, 467–480.

9 R. Duncan, *Nat. Rev. Cancer*, 2006, **6**, 688–701.

10 W. Xu, J. Ding, C. Xiao, L. Li, X. Zhuang and X. Chen, *Biomaterials*, 2015, **54**, 72–86.

11 J. Zou, F. Zhang, S. Zhang, S. F. Pollack, M. Elsabahy, J. Fan and K. L. Wooley, *Adv. Healthcare Mater.*, 2014, **3**, 441–448.

12 Y. Yu, C.-K. Chen, W.-C. Law, E. Weinheimer, S. Sengupta, P. N. Prasad and C. Cheng, *Biomacromolecules*, 2014, **15**, 524–532.

13 R. K. O'Reilly, C. J. Hawker and K. L. Wooley, *Chem. Soc. Rev.*, 2006, **35**, 1068–1083.

14 Q. Hu, C. J. F. Rijcken, E. van Gaal, P. Brundel, H. Kostkova, T. Etrych, B. Weber, M. Barz, F. Kiessling, J. Prakash, G. Storm, W. E. Hennink and T. Lammers, *J. Controlled Release*, 2016, **244**, 314–325.

15 Y. Li, K. Xiao, W. Zhu, W. Deng and K. S. Lam, *Adv. Drug Delivery Rev.*, 2014, **66**, 58–73.

16 J. Ding, L. Chen, C. Xiao, L. Chen, X. Zhuang and X. Chen, *Chem. Commun.*, 2014, **50**, 11274–11290.

17 L. Wu, Y. Zou, C. Deng, R. Cheng, F. Meng and Z. Zhong, *Biomaterials*, 2013, **34**, 5262–5272.

18 C.-C. Cheng, F.-C. Chang, H.-C. Yen, D.-J. Lee, C.-W. Chiu and Z. Xin, *ACS Macro Lett.*, 2015, **4**, 1184–1188.

19 Y. Liang, X. Deng, L. Zhang, X. Peng, W. Gao, J. Cao, Z. Gu and B. He, *Biomaterials*, 2015, **71**, 1–10.

20 Y. Shi, R. van der Meel, B. Theek, E. O. Blenke, E. H. E. Pieters, M. H. A. M. Fens, J. Ehling, R. M. Schiffelers, G. Storm, C. F. van Nostrum, T. Lammers and W. E. Hennink, *ACS Nano*, 2015, **9**, 3740–3752.

21 O. P. Varghese, J. Liu, K. Sundaram, J. Hilborn and O. P. Oommen, *Biomater. Sci.*, 2016, **4**, 1310–1313.

22 B. Sun, C. Deng, F. Meng, J. Zhang and Z. Zhong, *Acta Biomater.*, 2016, **45**, 223–233.

23 T. J. Deming, *Chem. Rev.*, 2016, **116**, 786–808.

24 C. He, X. Zhuang, Z. Tang, H. Tian and X. Chen, *Adv. Healthcare Mater.*, 2012, **1**, 48–78.

25 H. Lu, J. Wang, Z. Song, L. Yin, Y. Zhang, H. Tang, C. Tu, Y. Lin and J. Cheng, *Chem. Commun.*, 2014, **50**, 139–155.

26 P. Mi, D. Kokuryo, H. Cabral, H. Wu, Y. Terada, T. Saga, I. Aoki, N. Nishiyama and K. Kataoka, *Nat. Nanotechnol.*, 2016, **11**, 724–730.

27 C. Deng, J. Wu, R. Cheng, F. Meng, H.-A. Klok and Z. Zhong, *Prog. Polym. Sci.*, 2014, **39**, 330–364.

28 M. H. Park, M. K. Joo, B. G. Choi and B. Jeong, *Acc. Chem. Res.*, 2012, **45**, 424–433.

29 X. Wu, Y. Wu, H. Ye, S. Yu, C. He and X. Chen, *J. Controlled Release*, 2017, **255**, 81–93.

30 G. J. M. Habraken, M. Peeters, P. D. Thornton, C. E. Koning and A. Heise, *Biomacromolecules*, 2011, **12**, 3761–3769.

31 J. Huang, C. L. Hastings, G. P. Duffy, H. M. Kelly, J. Raeburn, D. J. Adams and A. Heise, *Biomacromolecules*, 2013, **14**, 200–206.

32 M. Qiu, J. Ouyang, H. Sun, F. Meng, R. Cheng, J. Zhang, L. Cheng, Q. Lan, C. Deng and Z. Zhong, *ACS Appl. Mater. Interfaces*, 2017, **9**, 27587–27595.

33 J. Huang, C. Bonduelle, J. Thevenot, S. Lecommandoux and A. Heise, *J. Am. Chem. Soc.*, 2012, **134**, 119–122.

34 K. Ren, Y. Cheng, C. He, C. Xiao, G. Li and X. Chen, *Polymer*, 2013, **54**, 2466–2472.

35 M. K. Joo, D. Y. Ko, S. J. Jeong, M. H. Park, U. P. Shinde and B. Jeong, *Soft Matter*, 2013, **9**, 8014–8022.

36 Y. Cheng, C. He, J. Ding, C. Xiao, X. Zhuang and X. Chen, *Biomaterials*, 2013, **34**, 10338–10347.

37 L. Waentig, N. Jakubowski, H. Hayen and P. H. Roos, *J. Anal. At. Spectrom.*, 2011, **26**, 1610–1618.

38 V. Tolmachev and S. Stone-Elander, *Biochim. Biophys. Acta, Gen. Subj.*, 2010, **1800**, 487–510.

39 E. A. Simone, B. J. Zern, A.-M. Chacko, J. L. Mikitsh, E. R. Blankemeyer, S. Muro, R. V. Stan and V. R. Muzykantov, *Biomaterials*, 2012, **33**, 5406–5413.

40 J. Wang, H. Zhao, Z. Zhou, P. Zhou, Y. Yan, M. Wang, H. Yang, Y. Zhang and S. Yang, *ACS Appl. Mater. Interfaces*, 2016, **8**, 19872–19882.

41 Y. Zou, Y. Wei, G. Wang, F. Meng, M. Gao, G. Storm and Z. Zhong, *Adv. Mater.*, 2017, **29**, 1603997.

42 L. Zhang, R. Zhang, J. Yang, J. Wang and J. Kopecek, *J. Controlled Release*, 2016, **235**, 306–318.

43 C. Tang, J. Edelstein, J. L. Mikitsh, E. Xiao, A. H. Hemphill II, R. Pagels, A.-M. Chacko and R. Prud'homme, *J. Mater. Chem. B*, 2016, **4**, 2428–2434.

44 J. Lv, H. Sun, Y. Zou, F. Meng, A. A. Dias, M. Hendriks, J. Feijen and Z. Zhong, *Biomater. Sci.*, 2015, **3**, 1134–1146.

45 K. Cai, X. He, Z. Song, Q. Yin, Y. Zhang, F. M. Uckun, C. Jiang and J. Cheng, *J. Am. Chem. Soc.*, 2015, **137**, 3458–3461.

46 P. Huang, D. Wang, Y. Su, W. Huang, Y. Zhou, D. Cui, X. Zhu and D. Yan, *J. Am. Chem. Soc.*, 2014, **136**, 11748–11756.

47 Y. Shen, E. Jin, B. Zhang, C. J. Murphy, M. Sui, J. Zhao, J. Wang, J. Tang, M. Fan, E. Van Kirk and W. J. Murdoch, *J. Am. Chem. Soc.*, 2010, **132**, 4259–4265.

48 Y. Cai, H. Shen, J. Zhan, M. Lin, L. Dai, C. Ren, Y. Shi, J. Liu, J. Gao and Z. Yang, *J. Am. Chem. Soc.*, 2017, **139**, 2876–2879.

49 Y. Shi, M. J. van Steenbergen, E. A. Teunissen, L. Novo, S. Gradmann, M. Baldus, C. F. van Nostrum and W. E. Hennink, *Biomacromolecules*, 2013, **14**, 1826–1837.

50 H. B. Ruttala, N. Chitrapriya, K. Kaliraj, T. Ramasamy, W. H. Shin, J.-H. Jeong, J. R. Kim, S. K. Ku, H.-G. Choi, C. S. Yong and J. O. Kim, *Acta Biomater.*, 2017, **63**, 135–149.

51 W. Cao, X. Zeng, G. Liu, Z. Li, X. Zeng, L. Wang, L. Huang, S.-S. Feng and L. Mei, *Acta Biomater.*, 2015, **26**, 145–158.

52 J. Li, Y. Qiao and Z. Wu, *J. Controlled Release*, 2017, **256**, 9–18.

53 J. Wu, C. Deng, F. Meng, J. Zhang, H. Sun and Z. Zhong, *J. Controlled Release*, 2017, **259**, 76–82.

54 G. Chinetti-Gbaguidi, S. Colin and B. Staels, *Nat. Rev. Cardiol.*, 2015, **12**, 10–17.

55 Y.-C. Liu, X.-B. Zou, Y.-F. Chai and Y.-M. Yao, *Int. J. Biol. Sci.*, 2014, **10**, 520–529.

56 C. Raggi, H. S. Mousa, M. Corrent, A. Sica and P. Invernizzi, *Oncogene*, 2016, **35**, 671–682.

57 M. C. Morrison and R. Kleemann, *Front. Immunol.*, 2015, **6**, 1–13.

58 Z. Li, H. Huang, S. Tang, Y. Li, X.-F. Yu, H. Wang, P. Li, Z. Sun, H. Zhang, C. Liu and P. K. Chu, *Biomaterials*, 2016, **74**, 144–154.

59 R. Firdessa, T. A. Oelschlaeger and H. Moll, *Eur. J. Cell Biol.*, 2014, **93**, 323–337.

60 Y. Zhong, F. Meng, C. Deng and Z. Zhong, *Biomacromolecules*, 2014, **15**, 1955–1969.

61 Q. Dai, Y. Yan, J. Guo, M. Bjoernmalm, J. Cui, H. Sun and F. Caruso, *ACS Macro Lett.*, 2015, **4**, 1259–1263.